# Orographic Enhancement of Rainfall Over the Congo Basin

Ajay Raghavendra<sup>1</sup>, Geng Xia<sup>2</sup>, Liming Zhou<sup>3</sup>, and Yan Jiang<sup>3</sup>

<sup>1</sup>U.S. Army, Latham, NY, USA

<sup>2</sup>National Wind Technology Center, National Renewable Energy Laboratory, Golden, CO, USA

<sup>3</sup>Department of Atmospheric and Environmental Sciences, University at Albany, Albany, NY,

USA

Submitted to Atmospheric Science Letters

Submitted on August 17, 2022 Revised on January 12, 2022 Accepted on January 13, 2022

**Citation**: Raghavendra, A., Xia, G., Zhou, L., Jiang, Y., 2022. Orographic enhancement of rainfall over the Congo Basin. *Atmospheric Science Letters*. 23(4), e1079. <a href="https://doi.org/10.1002/asl.1079">https://doi.org/10.1002/asl.1079</a>

#### Abstract

The Congo rainforest located in central equatorial Africa is an important, yet understudied part of the globe surrounded by complex orographic features. A primitive understanding of precipitation processes such as mesoscale convective dynamics magnifies uncertainties in the future climate projections of the hydrological cycleover the Congo. Furthermore, the effects of orography, which is an important forcing for convection and precipitation, are poorly resolved by climate models, and ill-conceptualized over the Congo. To address this knowledge gap, perturbed orographic forcing experiments are conducted using the Weather Research and Forecasting (WRF) mesoscale numerical model in a high-resolution convection-permitting model setup. The model simulated selected dates in November 2014. The thunderstorms and rainfall simulated in the control run for the case study analyzed in this paper compared reasonably-well to satellite derived brightness temperature and rainfall data. The results from this case study show that the dynamical impact of increasing the height of the East African Highlands is the blocking of the lower-tropospheric tropical easterlies. This weakening of the lower-tropospheric zonal winds increases the windshear over the Congo Basin resulting in slower propagating, more intense mesoscale convective systems with enhanced rainfall.

#### 1. Introduction

The second largest and one of the most understudied rainforests of the world i.e., the Congo located in equatorial Africa is also the driest (rainfall totaling ~1500 mm yr¹) when compared to other major rainforests (Alsdorf et al., 2016; Zhou et al., 2014). The Congo rainforest exists despite the significantly lower rainfall amount, is an important influence in the global carbon cycle, and particularly vulnerable to climate change (Haensler et al., 2013; Malhi et al., 2013). Unfortunately, the general circulation models (GCMs) used in the Coupled Model Intercomparison Project Phase 5 (CMIP5; Taylor et al., 2012) produce a large spread in the historic and future climate projections of precipitation over the Congo basin (e.g., Haensler et al., 2013; Washington et al., 2013). Some of these uncertainties may be attributable to the coarse representation of orography (Fig. 1) and mesoscale convective dynamics (e.g., Chen and Dai 2019; Dai 2006) in low-resolution datasets.

Over the Congo, there is still considerable debate on what role topographical features such as the Ethiopian highlands, Turkana channel, and East African Highlands play in channeling moisture into the Congo (e.g., Dyer et al., 2017; Sorí et al., 2017), and whether these orographic features surrounding the Congo work to enhance or suppress thunderstorm activity and rainfall. From a dynamic perspective, orography plays a profound role as an atmospheric forcing. For instance, atmospheric flow over a mountain may result in atmospheric wave activity, flow blocking, cyclogenesis (lee cyclogenesis, e.g., Pontoppidan et al., 2019), and precipitation enhancement or suppression (e.g., Sotillo et al., 2003). The persistent easterly low-level jet and associated moisture transport overthe African highlands (e.g., King et al. 2021; Munday et al. 2021) further motivates the investigation of orographic enhancement of rainfall over the Congo. Other factors that encourage the study of orography include micrometeorological constraints such as sunlight availability for photosynthesis and evapotranspiration over mountainous regions (e.g., Motzer 2005, Crowhurst et al. 2021).

The Congo basin is often regarded as a "convective engine" of the global atmospheric circulation and is the world's foremost lightning hotspot (Malhi et al., 2013). Furthermore, mesoscale convective systems (MCSs) are the primary source for rainfall across tropical Africa (Jackson et al., 2009; Taylor et al., 2018). While large scale influences of Africa's orography have been investigated to understand the south east Asian Monsoon (Wie and Bordoni 2016), and the influence of the East African highlands on the atmospheric circulation, temperature and rainfall over Africa have been evaluated using numerical models (e.g., Slingo et al., 2005; Sommerfeld et al. 2016), many unanswered questions pertaining to mechanisms for MCS activity and rainfall over the Congo persist. Jackson et al. (2009) inferred that the interannual variability in convection and MCS activity over the Congo Basin is dictated by changes in the interaction between wind speed and local topography over time. But the association between rainfall and topography was based on empirical analyses of satellite observations and reanalysis data, which cannot directly clarify causality. This paper seeks to narrow the knowledge gap by establishing a clearer understanding of the role that African orography plays in modulating thunderstorm activity and rainfall over the Congo. In this study, a high-resolution convection-permitting mesoscale numerical modeling framework is invoked. Since orography is the only perturbed field in such an experiment, changes in the atmosphere, thunderstorms, and rainfall characteristics may be predominantly attributable to orographic

# 2. Model Setup

Geostationary Infrared (IR) 11µm channel brightness temperature (Tb) data derived from GridSat-B1 satellite data (Knapp et al., 2011) show that MCSs were present on 05-Nov-2014 with a particularly large spatial extent over the Congo Basin (see OBS in Fig. 2), that contained both large and small convective cells characterized by cold cloud top temperatures. Intense tropical thunderstorms are generally characterized by colder cloud top temperatures, and vice versa (Raghavendra et al. 2018). This event was selected as the case study in the paper asit is a typical representation of MCS activity over the basin in November, which is the month with the strongest relationship between lower tropospheric easterlies and thunderstorm activity over the Congo. The data show that a few isolated and relatively weak thunderstorm cells (with relatively warm cloud top temperatures) propagated westward over the East African Highlands and entered the lowlands of the Congo basin between 00:00-06:00 UTC on 05-Nov (available through the GIBBS archive). Once over the Congo basin, these thunderstorm cells organized to form a large, quasi-linear shaped MCS between 12:00–18:00 UTC. On 06-Nov between the hours of 03:00–12:00 UTC, the MCS was observed to dissipate.

The NCAR Weather Research and Forecasting (WRF) Advanced Research WRF (WRF-ARW) model version 3.6.1 (Skamarock et al., 2008) was tested to assess whether it was able to successfully capture this typical mesoscale convective event (e.g., Laing et al. 2011). The model configuration for the simulations utilized the ARW-WRF version 3.6.1 run as a compressible, nonhydrostatic, and three-dimensional mesoscale model. The model was initialized with the European Centre for Medium-Range Weather Forecast (ECMWF) interim reanalysis (ERA-I; Dee et al., 2011) data at 00:00 UTC 02-Nov-2014 and ran continuously without spectral nudging for 120 hours (i.e., simulation ends on 00:00 UTC 07-Nov-2014) using a large domain [1300 (latitude) × 700 (longitude) grid points] at 4 km horizontal resolution centered around the Congo basin (Fig. 1a). The first 48 hours were reserved for model stabilization and spin-up, and a detailed evaluation of the simulations is presented from 12:00 UTC 05-Nov to 12:00 UTC 06-Nov. The simulation used 38 vertical levels with the finest resolution in the planetary boundary layer (PBL) and incorporated the following parameterization schemes which closely follows Rasmussen and Houze (2016): Longwave Radiation: Rapid Radiative Transfer Model (Mlawer et al., 1997), Shortwave Radiation: Dudhia (Dudhia 1989), Surface Layer: Revised MMR surface layer scheme (Jimenez et al., 2012), Microphysics: Thompson 6-class scheme with graupel and double moment for cloud ice, (Thompson et al., 2008), Land Surface: Noah Land Surface (Chen and Dudhia 2001), and PBL: Yonsei University PBL (Hong et al., 2006). Given the relatively high horizontal resolution, convection was explicitly resolved, and a cumulus parameterization scheme was not invoked.

Three simulations including the control run (CTL) were conducted using the ARW-WRF model. The CTL run followed the model setup previously described in this section and utilized the USGS (U.S. Geological Survey)topography and land classification. Two perturbation runs were setup in a manner identical to the CTL run with the exception of the input orography file. The model run with a 50% lower orography (TOPO<sub>50%</sub>) compared to the CTL was supplied with a modified topography file where the African orography was multiplied by 0.5 and

smoothened once using 10 grid points in each direction. The result closely resembles the input orography file for a typical GCM (Fig. 1b). On the other hand, the model run with a 50% higher orography (TOPO150%) compared to the CTL was supplied with a modified topography file where the African orography was multiplied by 1.5. The differences in the topographical input for the three model runs may be visualized in Fig. 2.

### 3. Model Validation

The WRF-derived outgoing longwave radiation (OLR) data were converted to brightness temperature using the Stefan-Boltzmann law to enable the WRF model data to be evaluated for accuracy against the GridSat-B1 data. Studying the spatial patterns and temporal evolution of the MCSs observed by the GridSat-B1 data, and MCSs and rainfall simulated by the WRF model provides snapshots to validate the CTL run. Fig. 2 shows the spatial extent and intensity of thunderstorm activity from the observations and three model runs for five timesteps. A qualitative analysis of the OBS and CTL images shows that the CTL run is able to reasonably reproduce the major features including the location, development, and propagation of thunderstorms from OBS. The NNW-SSE oriented quasi-linear squall line over the Congo at 12:00 UTC on 05-Nov in the OBS is simulated with a WNW-ESE orientation in the CTL run. At 18:00 UTC on 05-Nov however, the MCSs are reasonably well captured in the CTL run. A single organized thunderstorm cluster located near the eastern edges of the Congo at 00:00 UTC on 06-Nov in the OBS is simulated as multiple scattered thunderstorm cells across the Congo in the CTL run. In both the OBS and CTL run, a significant reduction in thunderstorm activity is observed between 00:00 and 06:00 UTC. This activity remains low between 06:00 and 12:00 UTC on 06-Nov. Some deviations from observations are expected in the CTL run since it is unrealistic to expect a model initialized and forced with a coarser resolution reanalysis data to reproduce observations without some degradation. Also, the WRF model is sensitivity to the choice of parameterization schemes, and spectral nudging which forces the WRF model output closer to the input data was not incorporated (e.g., Stratton et al., 2018).

Hovmöller diagrams (Fig. 3a–c and Fig. 3e–g) were constructed to further evaluate the CTL run against the satellite observations. Unlike the spatial comparison of thunderstorms in Fig. 2, the Hovmöller diagram allows for the comparison of timing and propagation characteristics of thunderstorms between the OBS and CTL run. The primary MCS analyzed in this study is shown in the OBS and CTL run starting at 12:00 UTC on 05-Nov near 22°E. The thunderstorm cells propagate westward and linearly in time starting from about 22°E to  $12^{\circ}$ E over a 24-hour period. The propagation characteristics of thunderstorms are similar between the OBS and CTL run, but some differences in the overall spatial structure of the thunderstorms are worth noting. In Fig. 3c, regions shaded in blue show convective activity in the CTL run that are absent in the observations and vice-versa for regions shaded in red. Overall, there is a significantly correlation (R = 0.86) in the time evolution of cold cloud between the OBS and CTL over the Congo (Fig. 3d). As in the OBS, the CTL run also reproduces the tropical diurnal cycle of thunderstorm activity over land (Fig. 3d).

Due to the sparse surface observation network over the Congo (Washington et al., 2013), calibrated precipitation estimates from the Integrated Multi-satellitE Retrievals for GPM (GPM IMERG Final Precipitation L3 Half Hourly  $0.1^{\circ} \times 0.1^{\circ}$  V06; Huffman et al., 2019a, b) was

also used for additional model validation (Fig. 3e–h). The high-resolution IMERG dataset may be directly used to validate the WRF output with minimal interpolation errors. Given the strong relationship between convective activity and rainfall, the differences in rainfall between the OBS and CTL run closely follow the differences in the spatial extent of convective activity (Fig. 3e–g). The time evolution of rainfall between the IMERG and CTL run was also significantly correlated (R = 0.64; Fig. 3h). In summary, Figs. 2–3 demonstrates that the WRF model performs reasonably well in capturing the MCSs which occurred between 05-Nov and 06-Nov-2014. Additional methods to validate the model output with observations would be challenging over the Congo due to the lack of high-frequency surface or air/space-borne observations (Washington et al., 2013; Alsdorf et al., 2016), and the inability to properly resolve mesoscale events and precipitation characteristics even in the latest high-resolution reanalysis products such as ERA-5.

# 4. Results

The orographic impacts on the circulation, thunderstorm and and precipitation between the CTL, TOPO50%, and TOPO150% runs are presented in this section. Results include the spatial extent and propagation characteristics of thunderstorm activity, rainfall, and the windfield structures. Differences in the vertical (height—longitude) crosssectional view of winds, specific humidity, and precipitation are also presented in this section.

# a) Spatial extent and intensity of thunderstorms and rainfall

Differences in the spatial extent of thunderstorms and their intensity between the three WRF model runs are illustrated in Fig. 2. At all timesteps, the TOPO<sub>50%</sub> run produces fewer and weaker thunderstorms, while the TOPO<sub>150%</sub> run is characterized by stronger and more intense thunderstorms. While the overall location of the thunderstorm cells in the three WRF model runs are similar, the spatial extent and intensity of thunderstorms show considerable differences. At 12:00 UTC and 18:00 UTC on 05-Nov, there are few differences in the spatial extent of thunderstorms between the CTL and TOPO<sub>150%</sub> runs while the thunderstorms in the TOPO<sub>50%</sub> run are considerably smaller. At 00:00 UTC on 06-Nov, most of the thunderstorms have moved away from the Congo basin and are located over the west-African coastline in the TOPO<sub>50%</sub> run. At the same time, thunderstorms persist in the CTL and TOPO<sub>150%</sub> runs. As typically observed for the tropical diurnal cycle over land, from 00:00 UTC to 12:00 UTC on 06-Nov, thunderstorms dissipate overnight and through the morning hours.

Tropical thunderstorm intensity may be assessed using cold cloud top temperatures (Raghavendra et al. 2018). The spatial extent, intensity, and propagation characteristics of thunderstorms in the CTL, TOPO<sub>50</sub>%, and TOPO<sub>150</sub>% runs may be further analyzed using Hovmöller diagrams in Fig. 4a–d and Fig. 5a–d. As in Fig. 2, the thunderstorms are large and more intense in the TOPO<sub>150</sub>% run when compared to the TOPO<sub>50</sub>% run. When compared to the CTL run, the spatial extent and intensity of thunderstorms in TOPO<sub>50</sub>% run are smaller. The dominance of warmer red shading in Fig. 4b shows that the thunderstorms in TOPO<sub>50</sub>% run are not as intense when compared to their CTL run counterparts. On the other hand, Fig. 4c–d shows that thunderstorms in the TOPO<sub>150</sub>% run are larger and more intense when compared to their CTL counterparts. Finally, the spatial extent of cold cloud top pixels shows fewer cold clouds in the TOPO<sub>50</sub>% when compared to the TOPO<sub>150</sub>% run (Fig. 4e).

Over the tropical latitudes, a strong relationship between convective activity and rainfall are expected (Dai 2006). In order to evaluate convective activity and rainfall, surface rainfall data are presented in Fig. 5. As expected, the spatial structure, intensity and difference in rainfall between the experimental runs (i.e., TOPO<sub>50%</sub> and TOPO<sub>150%</sub> runs) and CTL run closely follow Fig. 4. Fig. 5b shows red streaks and Fig. 5d shows blue streaks indicative of reduced rainfall in the TOPO<sub>50%</sub> run and enhanced rainfall in the TOPO<sub>150%</sub> run when compared to the CTL run. Fig. 5f shows that the total accumulated rainfall over the Congo is largest for the TOPO<sub>150%</sub> (~26 mm) and smallest for the TOPO<sub>50%</sub> run (~13 mm).

### b) Vertical Windshear

Vertical windshear is an important ingredient for the maintenance and longevity of an MCS (e.g., Chen et al., 2015; Taylor et al., 2018). The time evolution of the mid- and lower-tropospheric horizontal winds are presented as a Hovmöller diagrams in Fig. 6. In Fig. 7, the zonal, meridional, and vertical windshear are analyzed quantitatively. The analysis is presented using geopotential height (km) instead of pressure-level (hPa) in order to contextualize the results against the background orography. The Hovmöller diagrams in Fig. 6 show a similar overall structure for the 5.3 km (approximately 500 hPa) winds for all three model runs. The lower tropospheric winds at 1.2 km (approximately 850 hPa) on the other hand show large magnitude differences in the zonal winds and structural differences in the meridional winds. The strength of the lower-level zonal winds is strongest in the TOPO50% run, and weakest in the TOPO150% run. The zonal and meridional windshear is strongest in the TOPO150% run when compared to the TOPO50% run.

Orography blocks the easterly flow at the lower levels (~2 km), but has little impact in the mid-levels (~5 km). The blocking of the lower-level winds produces larger windshear in the TOPO150% run when compared to the TOPO50% run. Figure 7 shows the basin-wide average zonal wind and meridional wind across the case study period at 5km and 2km. In the mid-levels, there is very little difference in the zonal windspeed amongst the CTL, TOPO50%, and TOPO150% runs (Fig. 7a). In the lower-levels however (Fig. 7b), the zonal winds hover between -8 to -10 ms<sup>-1</sup> in the TOPO50% run and between 0 to -4 ms<sup>-1</sup> in the TOPO150% run. Orography acts to drastically reduces the zonal windspeed and thus enhancing the vertical windshear. The mid- (Fig. 7c) and lower- (Fig. 7d) levels meridional winds do not show any substantial spread between the three model runs and are weaker when compared to their zonal wind counterparts.

For the period 12:00 UTC 05-Nov to 12:00 UTC 06 Nov, the magnitude of the time mean zonal windshear for the TOPO<sub>50%</sub> run is 1.0 ms<sup>-1</sup>, and TOPO<sub>150%</sub> run is 4.9 ms<sup>-1</sup>. This result points to a mean increase of 3.9 ms<sup>-1</sup> in the zonal windshear between the low and high orography runs (Fig. 7a-b). On the other hand, the magnitudes of the time mean meridional windshear is 2.2 ms<sup>-1</sup> for the TOPO<sub>50%</sub> run and is 3.1 ms<sup>-1</sup> TOPO<sub>150%</sub> run. This resultsin a small increase in the mean meridional windshear by 0.9 ms<sup>-1</sup> with higher orography (Fig. 7c-d). At the mid-levels (solid line in Fig. 7e), there is a narrow spread in the mean wind speed between the three runs and ranges between 7.7 to 8.0 ms<sup>-1</sup>. However, the mean wind speed for the lower level (dashed line in Fig. 7e) for the three runs shows a larger spread and ranges between 3.1 to 8.8 ms<sup>-1</sup>. The TOPO<sub>50%</sub> produces the weakest mean verticalwindshear of -1.0 ms<sup>-1</sup>, while

the TOPO<sub>150%</sub> run produces the strongest mean vertical windshear of 4.2 ms<sup>-1</sup> (Fig.7f).

# c) Vertical cross-sectional analysis

Since the magnitude of the zonal wind is more than double when compared to the meridional wind, a longitude-height cross-sectional analysis by averaging 10 latitude points (40 km) across the equator for zonal and vertical winds, the rain/ice particle number concentration, and surface rainfall are presented in Fig. 8. The most pronounced differences between the CTL, TOPO<sub>50%</sub>, and TOPO<sub>150%</sub> runs are the intensity and diameter of the precipitation shaft, and the strength and propagation of the convective updrafts and downdrafts. The TOPO<sub>150%</sub> run is characterized by a stronger and wider precipitation shaft, and consequently produces the largest surface rainfall amounts when compared to the TOPO<sub>50%</sub> run. As shown in section 4b, the strong vertical windshear in the TOPO<sub>150%</sub> run when compared to the TOPO<sub>50%</sub> run may assist in the overall strength and longevity of these thunderstorms (e.g., Marion and Trapp 2019). The enhanced MCS and rainfall in the TOPO<sub>150%</sub> run when compared to the TOPO<sub>50%</sub> run may also be attributable to the de-coupling of the thunderstorm updraft downdraftpair as a result of strong orographically forced vertical windshear. The strong vertical windshear delays the weakening of the updraft by the downdraft by decoupling of the thunderstorm updraft downdraft pair during themature phases of the thunderstorm's lifecycle. Therefore, the lifecycle of the thunderstorm is prolonged and allows the thunderstorm to potentially evolve into a complex and well organized MCS (e.g., Marion and Trapp 2019).

These intense thunderstorm cells in the TOPO<sub>150%</sub> run also produces higher rainfall amounts while the TOPO<sub>50%</sub> run produces lesser rainfall (Fig. 5). Reinforcing the larger rainfall amounts in the TOPO<sub>150%</sub> run is the slower propagation speed of the rain shaft when compared to the TOPO<sub>50%</sub> run. The lower rainfall in the TOPO<sub>50%</sub> run leads in time whereas the higher rainfall in the TOPO<sub>150%</sub> run lags in time when compared to the CTL run (e.g., Fig. 2 at 00:00 UTC 06-Nov). The differences in the propagation speed of thunderstorms between the threemodel runs may be explained by studying the lower tropospheric zonal winds (Fig. 6–7). The faster zonal winds in the TOPO<sub>50%</sub> run helps steer the thunderstorms cells relatively quickly across the Congo basin.

### 5. Concluding Remarks

### a) Conclusion

In this study, a large MCS event over equatorial Africa is simulated using WRF at a convection-allowing resolution to investigate the dynamic aspects of perturbing orography. Given the poor representation of orography in GCMs (Fig. 1), the purpose of this study is to fill an important knowledge gap by highlighting the important relationship between African orography and rainfall over the Congo basin. While the complex orographic features surrounding the Congo basin have been suggested to play some role in modulating thunderstorms and rainfall (Jackson et al., 2009), the physical mechanisms have not been previously investigated. This work provides a dynamic assessment of orography, and the overall results complement previous studies such as Slingo et al. (2005), Jackson et al. (2009) and Sommerfeld et al. (2016). The dynamical impact of the African orography includes blocking of the tropical easterlies, which increasing the vertical windshear. The increase in

lower-level wind convergence in an already moist tropical environment may enhance the low-level moisture flux convergence, which is an important ingredient for thunderstorm activity (e.g., Cloutier-Bisbee et al., 2019). In summary, the dynamical impact of raising the orography of the East African highlands in this case study is a weakening of the lower-tropospheric zonal wind, that results in: 1) an increase in the vertical wind shear producingwell-sheared and intense MCSs, 2) slower propagation speed for the MCSs, and 3) rainfall enhancement over the Congo Basin.

# b) Possible future work

The Congo basin acts as a catchment zone, and the complex orography and vegetation distribution making up the Congo basin (Runge 2007; Alsdorf et al., 2016) results in substantial differences between the Congo river basin (watershed) and the Congo rainforest. The watershed is larger and includes nine riparian countries, including the relatively arid southern Congo basin. The rainforest on the other hand refers to the region that encompasses the humid tropical region with higher rainfall amount (Runge 2007; Alsdorf et al., 2016). Therefore, the spatial distribution of rainfall plays an important role in determining the hydrology (e.g., water table, soil moisture, and run off) and ecology of the Congo basin. Therefore, investigating the complex relationship between the spatial distribution of thunderstorm activity, rainfall and vegetation could potentially lead to a better understanding of the observed long-term drying trend and future of the Congo rainforest. These hydrological properties of the Congo basin could be further investigated by using models such as WRF-Hydro® (Gotchis et al. 2020).

Finally, improving the horizontal resolution and the representation of orography in GCMs (e.g., Chen and Dai 2019; Dai 2006), or incorporating high-resolution regional climate models (e.g., Future Climate for Africa FCFA, Improving Model Processes for African Climate -IMPALA project; Stratton et al., 2018) will significantly improve our understanding of the hydrological cycle and reduce uncertainties of future climate projections over the Congo. Future work may include the statistical and composite analysis using the IMPALA data to identify mechanisms (e.g., low-level jet, thermodynamic stability, and windshear) responsible for high and low convective events for each season for both the present and future climates. Changes linked to perturbing orography also result in microphysical changes such as the orographic seeder-feeder mechanism (e.g., Wilson and Barros 2014) which act to enhance rainfall could be analyzed in future studies. Finally, improving the horizontal resolution and the representation of orography in GCMs (e.g., Chen and Dai 2019; Dai 2006), or using highresolution regional climate models (e.g., CP4-Africa data from the IMPALA project; Stratton et al., 2018) could significantly improve our understanding of the hydrological cycle and reduce uncertainties of future climate projections over the Congo. The CP4-Africa could be used to identify mechanisms (e.g., low-level jet, thermodynamic stability, and windshear) responsible for generating intense MCS's in each season for both present and future climates.

# Acknowledgments

This work is supported by the National Science Foundation (NSF AGS-1535426 and AGS-1854486). All datasetsused in this study are free and publicly available: The ERA-I dataset is available from the ECMWF website <a href="mailto:ecmwf.int">ecmwf.int</a>, The GridSat-B1 data may be accessed from NOAA NCEI THREDDS Data Server (<a href="mailto:ncei.noaa.gov/thredds/satellite/gridsat\_b1.html">ncei.noaa.gov/thredds/satellite/gridsat\_b1.html</a>), and

the IMERG data may be accessed from NASA's website <u>doi.org/10.5067/GPM/IMERG/3B-HH/06</u>. Satellite images for this case study are available from the GIBBS archive <u>ncdc.noaa.gov/gibbs/html/MSG-3/IR/2014-11-05-00</u>. The constructive comments from two anonymous reviewers significantly improved this manuscript.

### References

- Alsdorf D, et al. (2016) Opportunities for hydrologic research in the Congo Basin. Rev. Geophys., 54: 378–409.
- Chen D, Dai A (2019) Precipitation Characteristics in the Community Atmosphere Model and Their Dependenceon Model Physics and Resolution, J. Adv. Model. Earth Sys., 11: 2352–2374.
- Chen Q, Fan J, Hagos S, Gustafson Jr WI, Berg LK (2015) Roles of wind shear at different vertical levels: Cloudsystem organization and properties. J. Geophys. Res. Atmos., 120: 6551–6574.
- Chen F, Dudhia J (2001) Coupling an advanced landsurface hydrology model with the Penn State/NCAR MM5modeling system. Part I: Model description and implementation. Mon. Wea. Rev., 129: 569–585.
- Cloutier-Bisbee SR, Raghavendra A, Milrad SM (2019) Heat Waves in Florida: Climatology, Trends, and RelatedPrecipitation Events. J. Appl. Meteor. Climatol, 58,:447–466.
- Crowhurst D, Dadson S, Peng J, Washington R (2021) Contrasting controls on Congo Basin evaporation at thetwo rainfall peaks. Clim. Dyn., 56: 1609–1624.
- Dai A (2006) Precipitation characteristics in eighteen coupled climate models. J. Climate, 19: 4605–4630.
- Dee DP, et al. (2011) The ERA-interim reanalysis: configuration and performance of the data assimilation system.Q. J. R. Meteo. Soc., 137: 553–597.
- Dudhia J (1989) Numerical study of convection observed during the winter monsoon experiment using a mesoscale twodimensional model. J. Atmos. Sci., 46: 3077–3107.
- Dyer ELE, et al. (2017) Congo Basin precipitation: assessing seasonality, regional interactions, and sources of moisture. J. Geophys. Res. Atmos., 122: 6882–6898.
- Gochis DJ, et al. (2020) The WRF-Hydro® modeling system technical description, (Version 5.1.1). NCAR Technical Note. 107 pp.
- Haensler A, Saeed F, Jacob D (2013) Assessment of projected climate change signals over central Africa based on a multitude of global and regional climate projections. In: Climate Change Scenarios for the Congo Basin.[A. Haensler, D. Jacob, P. Kabat, F. Ludwig (eds.)]. Climate Service Centre Report No. 11, Hamburg, Germany, ISSN: 2192-4058.
- Hong S-Y, Noh Y, Dudhia J (2006) A new vertical diffusion package with an explicit treatment of entrainment processes. Mon. Wea. Rev., 134: 2318–2341.
- Huffman GJ, Bolvin DT, Nelkin EJ, Tan J (2019a) Integrated Multi-satellitE Retrievals for GPM (IMERG) Technical Documentation. NASA GSFC, 77 pp.
- Huffman GJ, Stocker EF, Bolvin DT, Nelkin EJ and Tan J (2019b) GPM IMERG Final Precipitation L3 Half Hourly 0.1 degree x 0.1 degree V06, Greenbelt, MD, Goddard Earth Sciences Data and Information Services Center (GES DISC), Accessed: [23-Jun-2020], doi: 10.5067/GPM/IMERG/3B-HH/06.
- Jackson B, Nicholson SE, Klotter D (2009) Mesoscale convective systems over western equatorial Africa and their relationship to large-scale circulation. Mon. Wea. Rev., 137:

- 1272-1294.
- Jiménez PA, Dudhia J, González-Rouco JF, Navarro J, Montávez JP, García-Bustamante E (2012) A Revised Scheme for the WRF Surface Layer Formulation. Mon. Wea. Rev., 140: 898–918.
- King JA, Engelstaedter S, Washington R, Munday C (2021) Variability of the Turkana low-level jet in reanalysis and models: Implications for rainfall. J. Geophys. Res. Atmos., 126: e2020JD034154.
- Knapp KR (2008) Scientific data stewardship of International Satellite Cloud Climatology Project B1 global geostationary observations. J. Applied Remote Sensing, 2:023548.
- Knapp KR, et al. (2011) Globally gridded satellite (GridSat) observations for climate studies. Bull. Amer. Meteor. Soc., 92: 893–907.
- Laing AG, Carbone RE, Levizzani V (2011) Cycles and Propagation of Deep Convection over Equatorial Africa. Mon. Wea. Rev., 139: 2832-2853.
- Malhi Y, Adu-Bredu S, Asare RA, Lewis SL, Mayaux P (2013) African rainforests: past, present and future. Philos. T. R. Soc. B, 368: 20120312.
- Marion GR, Trapp RJ (2019) The dynamical coupling of convective updrafts, downdrafts, and cold pools in simulated supercell thunderstorms. J. Geophys. Res. Atmos., 124: 664–683.
- Mlawer EJ, Taubnam SJ, Brown PD, Iacono MJ, Clough SA (1997) Radiative transfer for inhomogeneous atmospheres: RRTM, a validated correlated-k model for the longwave. J. Geophys. Res., 102, 16663–16682.
- Motzer T (2005) Micrometeorological aspects of a tropical mountain forest. Agricultural and Forest Meteorology,135: 230–240.
- Munday C, Washington R, Hart N (2021). African low-level jets and their importance for water vapor transport and rainfall. Geophys. Res. Lett., 48:e2020GL090999.
- Pontoppidan M, Kolstad EW, Sobolowski SP, Sorteberg A, Liu C, Rasmussen RM (2019) Large-scale regional model biases in the extratropical North Atlantic storm track and impacts on downstream precipitation. Q. J. R.Meteor. Soc., 145: 2718–2732.
- Raghavendra A, Zhou L, Jiang Y, Hua W (2018) Increasing extent and intensity of thunderstorms observed overthe Congo Basin from 1982 to 2016. Atmos. Res., 213:17–26.
- Rasmussen KL, Houze Jr. RA (2016) Convective initiation near the Andes in subtropical South America. Mon. Wea. Rev., 144: 2351–2374.
- Runge J (2007) The Congo River, Central Africa, in Large Rivers: Geomorphology and Management, edited by A. Gupta, chap. 14, pp. 293–309, Wiley, U. K.
- Skamarock WC, et al. (2008) A description of the Advanced Research WRF version 3. NCAR Tech. NoteNCAR/TN-475+STR, 113 pp., doi: https://doi.org/10.5065/D68S4MVH.
- Slingo J, Spencer H, Hoskins B, Berrisford P, Black E (2005) The meteorology of the western Indian Ocean, and the influence of the East African Highlands. Philos. Trans. Roy. Soc. London A., 363: 25–42.
- Sommerfeld A, Prömmel K, Cubasch U (2016) The East African Rift System and the impact of orographic announce on regional climate and the resulting aridification. Int. J. Earth Sci., 105: 1779–1794.
- Sorí R, Nieto R, Vicente-Serrano SM, Drumond A, Gimeno L (2017) A Lagrangian perspective of thehydrological cycle in the Congo River basin. Earth Syst. Dynam., 8: 653–675.
- Sotillo MG, Ramis C, Romero R, Alonso S, Homar V (2003) Role of orography in the spatial distribution of precipitation over the Spanish Mediterranean zone. Climate Res., 23:

- 247-261.
- Stratton RA, et al. (2018) A Pan-African Convection-Permitting Regional Climate Simulation with the Met OfficeUnified Model: CP4-Africa. J. Climate, 31: 3485–3508.
- Taylor KE, Stouffer RJ, Meehl GA (2012) An overview of CMIP5 and the experiment design. Bull. Amer. Meteor. Soc., 93: 485–498.
- Taylor CM, et al. (2018) Earlier seasonal onset of intense Mesoscale Convective Systems in the Congo Basin since 1999. Geophys. Res. Lett., 45: 13458–13467.
- Thompson G, Field PR, Rasmussen RM, Hall WD (2008) Explicit forecasts of winter precipitation using an improved bulk microphysics scheme. Part II: Implementation of a new snow parameterization. Mon. Wea. Rev., 136, 5095–5115.
- Washington R, James R, Pearce H, Pokam WM, Moufouma-Okia W (2013) Congo Basin rainfall climatology: can we believe the climate models? Phil. Trans. Roy. Soc. B., 368: 20120296.
- Wei H-H, Bordoni S (2016) On the Role of the African Topography in the South Asian Monsoon. J. Atmos. Sci.,73: 3197–3212.
- Wilson AM, Barros AP (2014) An investigation of warm rainfall microphysics in the southern Appalachians: Orographic enhancement via low-level seeder–feeder interactions. J. Atmos. Sci., 71: 1783–1805.
- Zhou L, et al. (2014) Widespread decline of Congo rainforest greenness in the past decade. Nature, 509: 86–90.

# **Figures**

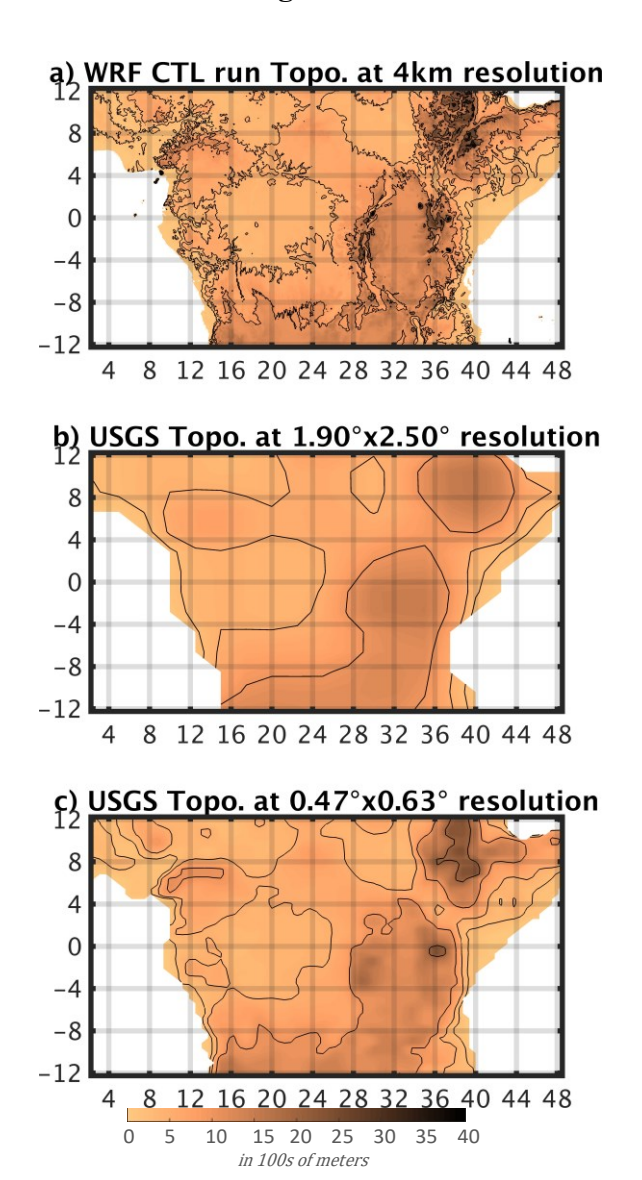


**Figure 1**. Topographical input data used in the a) WRF CTL run presented in this study, b) a typical GCM (e.g.,CMIP5 models), and c) a higher-resolution GCM.

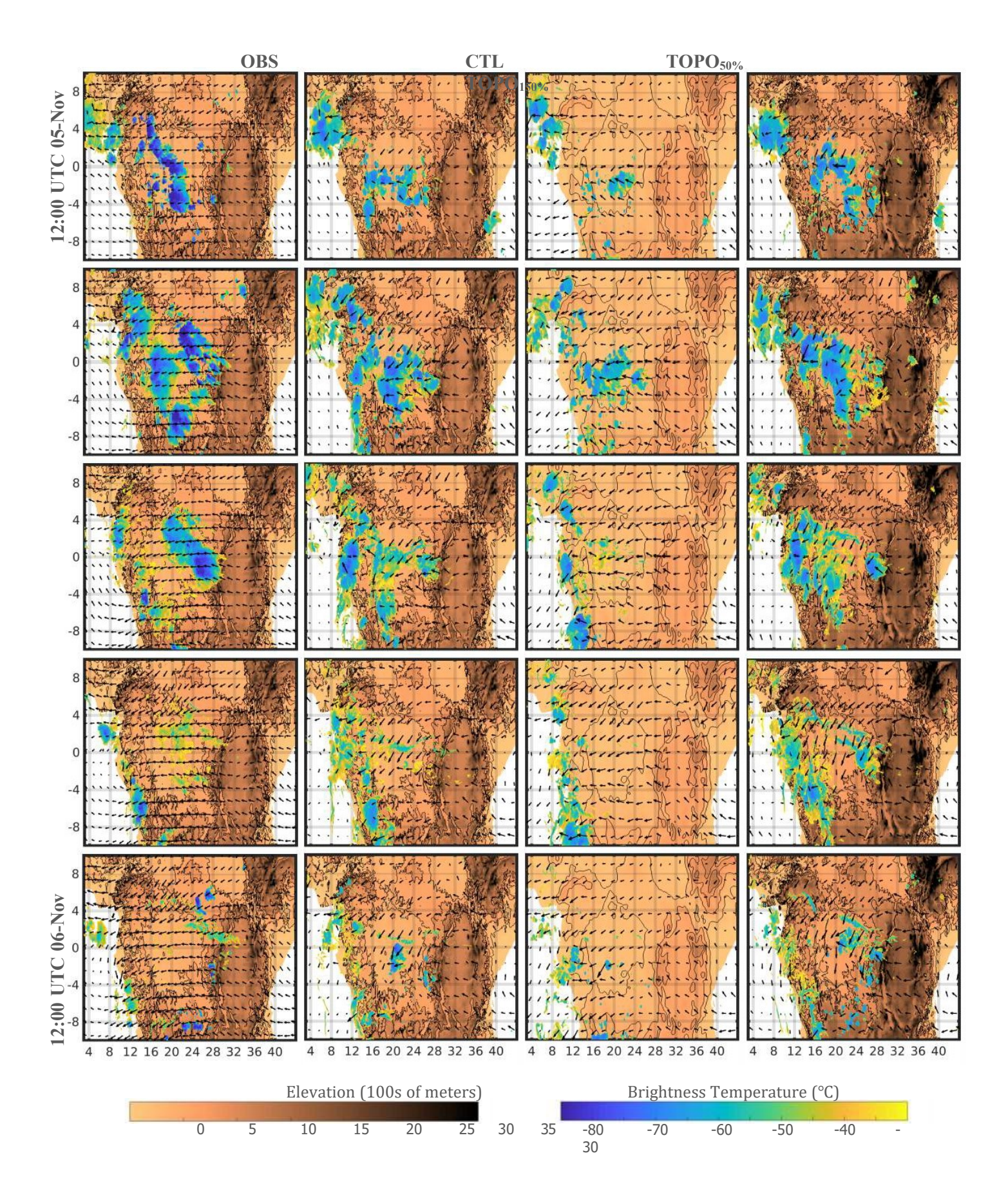


**Figure 2**. The evolution of MCSs diagnosed using cold cloud top brightness temperature (T!) over equatorial Africa shown every 6-h from 12:00 UTC on 05-Nov to 12:00 UTC on 06-Nov 2014 from GridSat-B1 (OBS), and CTL, TOPO"#% and TOPO%"#% runs. Zonal and meridional wind vectors from ERA-I (800 to 500 hPa layer mean for OBS) and the WRF model (2 to 5 km layer mean) are also displayed. Color bars for orography (in 10% meters) and T! (in C) are displayed below the figure.

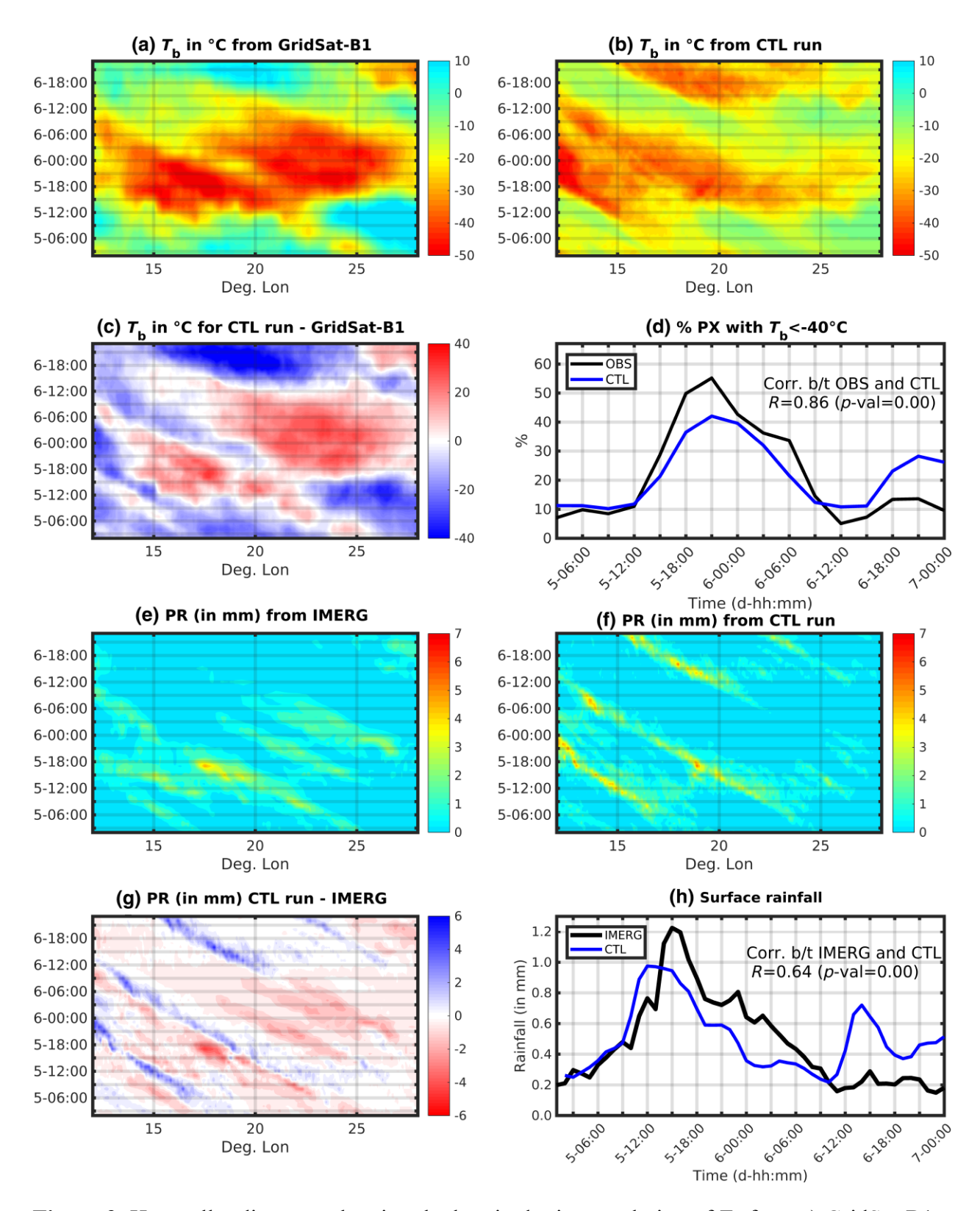


**Figure 3**: Hovmöller diagrams showing the longitude-time evolution of  $T_1$  from a) GridSat-B1, b) CTL run, and CTL run — GridSat-B1. d) Spatial extent of cold cloud pixels (PX) from the CTL run and GridSat-B1. Rainfall from e) IMERG, f) CTL run, and g) CTL run — IMERG. h)

Spatially averaged hourly rainfall from the CTL run and IMERG. All data were spatially averaged between  $5^{\circ}N/S$ , and between  $12^{\circ}$  and  $28^{\circ}$  for panel e.

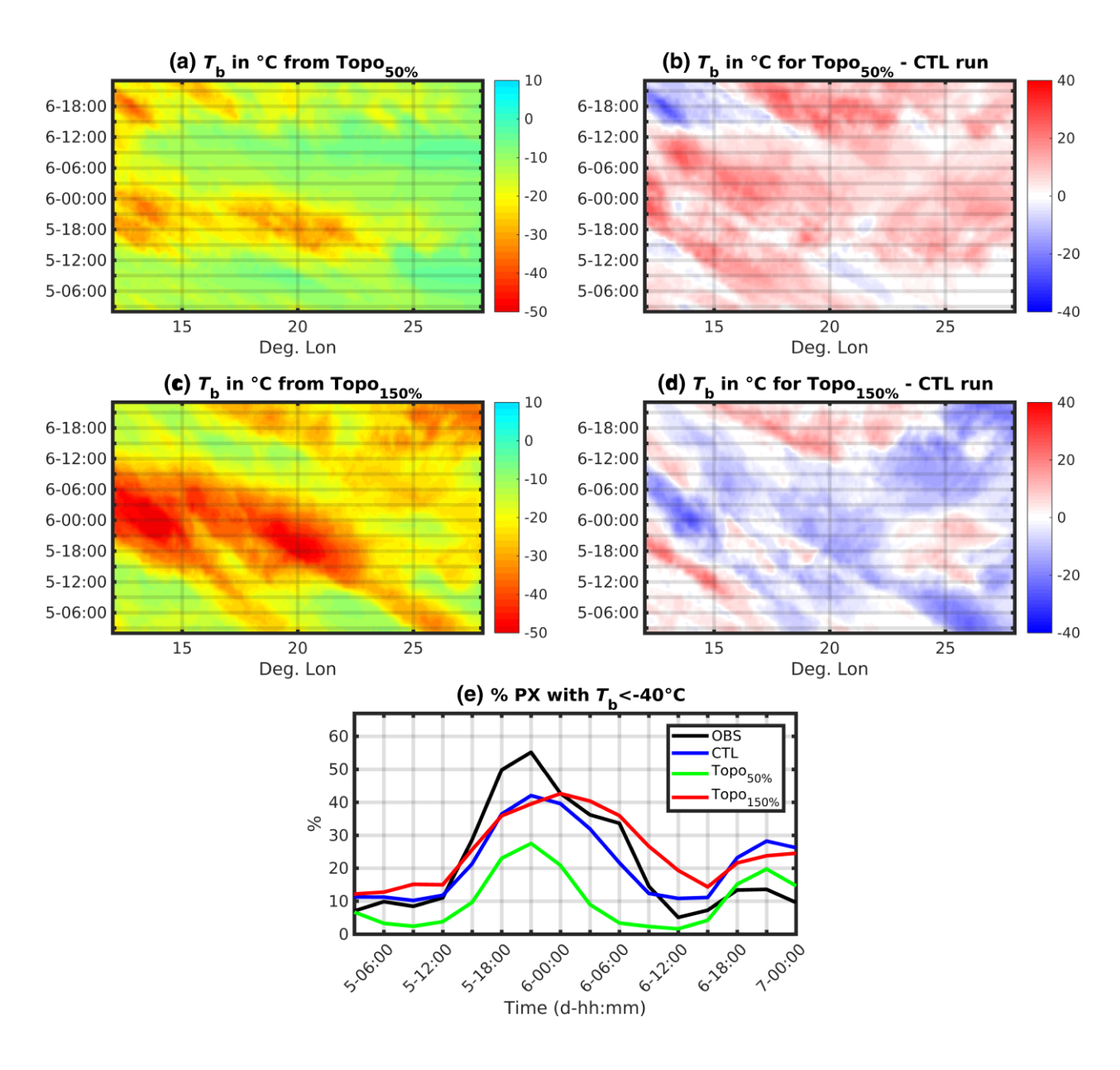


**Figure 4**: Hovmöller diagrams showing the longitude-time evolution of  $T_!$  from a)  $TOPO^*_{\#\%}$  run, b)  $TOPO^*_{\#\%} - CTL$  run, c)  $TOPO^*_{\#\%}$  run, and d)  $TOPO^*_{\#\%} - CTL$  run. e) Spatially averaged  $T_!$  from GridSat-B1, CTL,  $TOPO^*_{\#\%}$ , and  $TOPO^*_{\#\%}$  runs. All data were spatially averaged between  $5^\circ N/S$ , and between  $12^\circ$  and  $28^\circ$  forpanel e.

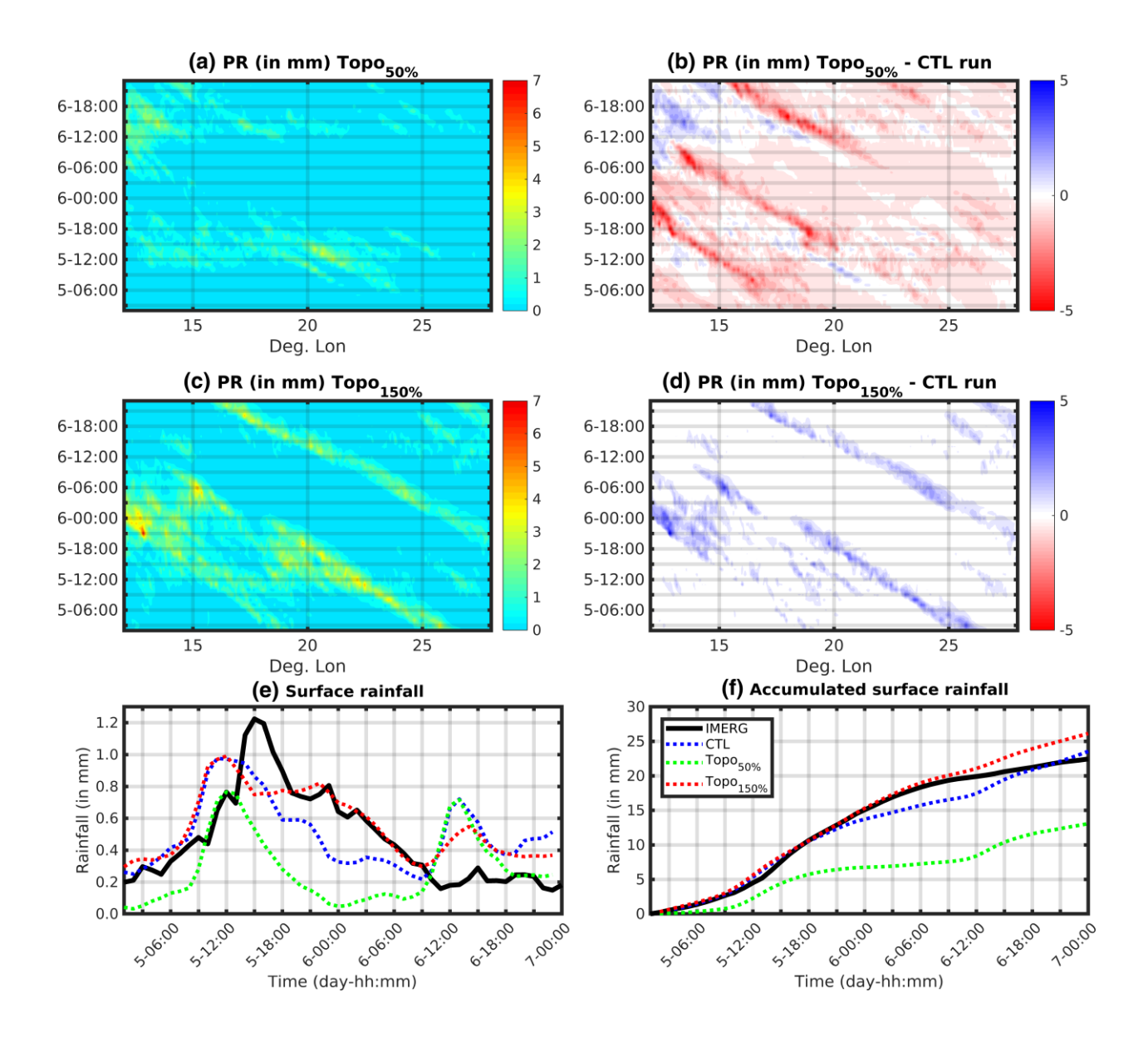


**Figure 5**: Hovmöller diagrams showing the longitude-time evolution of rainfall from a) TOPO"#% run, b) TOPO"#% - CTL run, c) TOPO%"#% run, and d) TOPO%"#% - CTL run. Spatially averaged e) hourly and f) accumulated rainfall from IMERG, CTL, TOPO"#%, and TOPO%"#% runs. All data were spatially averaged between 5°N/S, and between 12° and 28° for panel e and f.

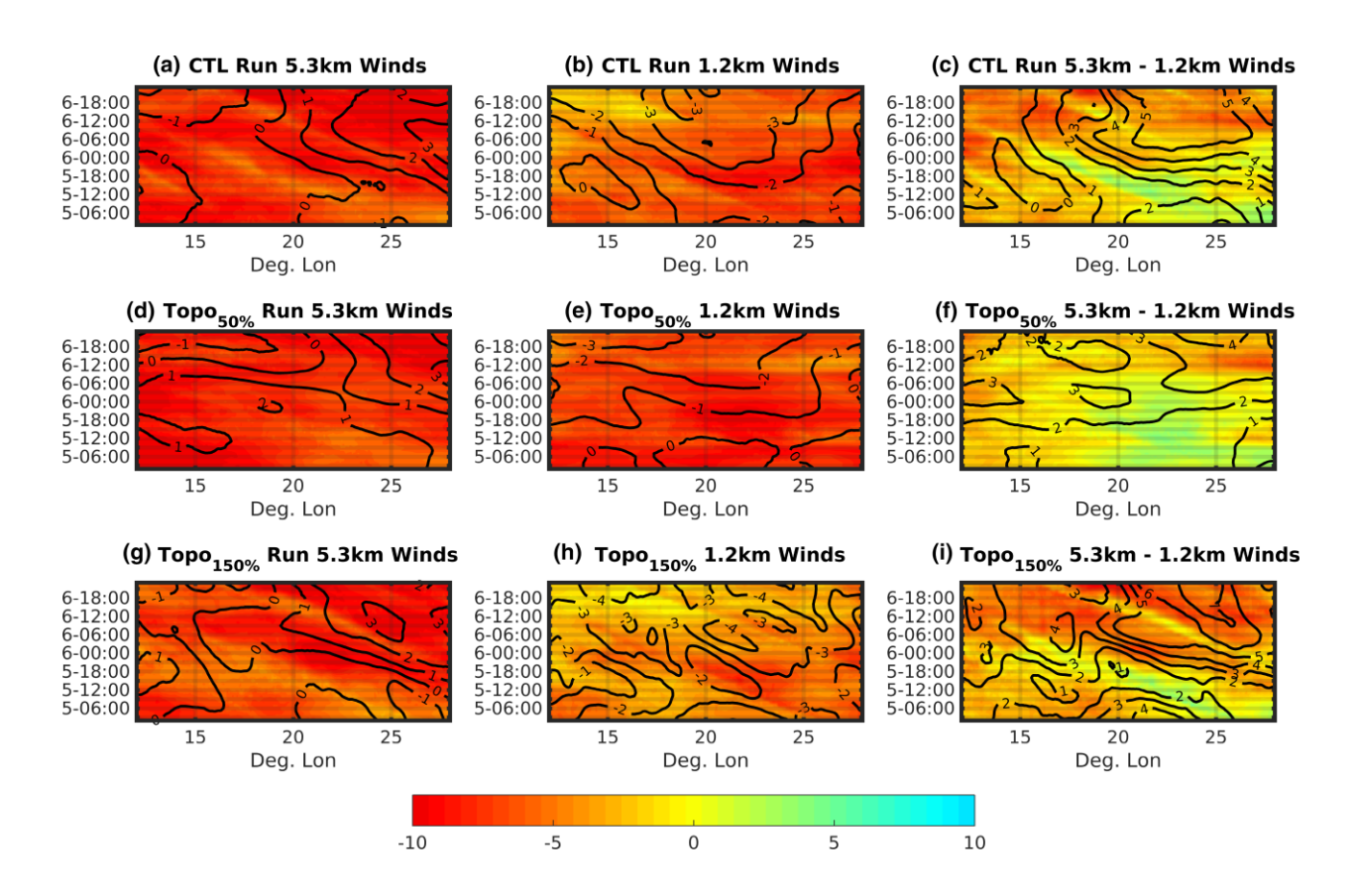


**Figure 6**: Hovmöller diagrams showing the longitude-time evolution of zonal (shaded;  $ms^{-1}$ %) and meridional (contoured;  $ms^{-1}$ %) winds from CTL run at a) 5.3 km, b) 1.2 km, and c) 5.3 km-1.2 km windshear. d-f) As in a – c but for the  $TOPO^{-1}$ % run. h-j) As in a – c but for the  $TOPO^{-1}$ % run. All data were spatially averaged between  $5^{\circ}N/S$ .

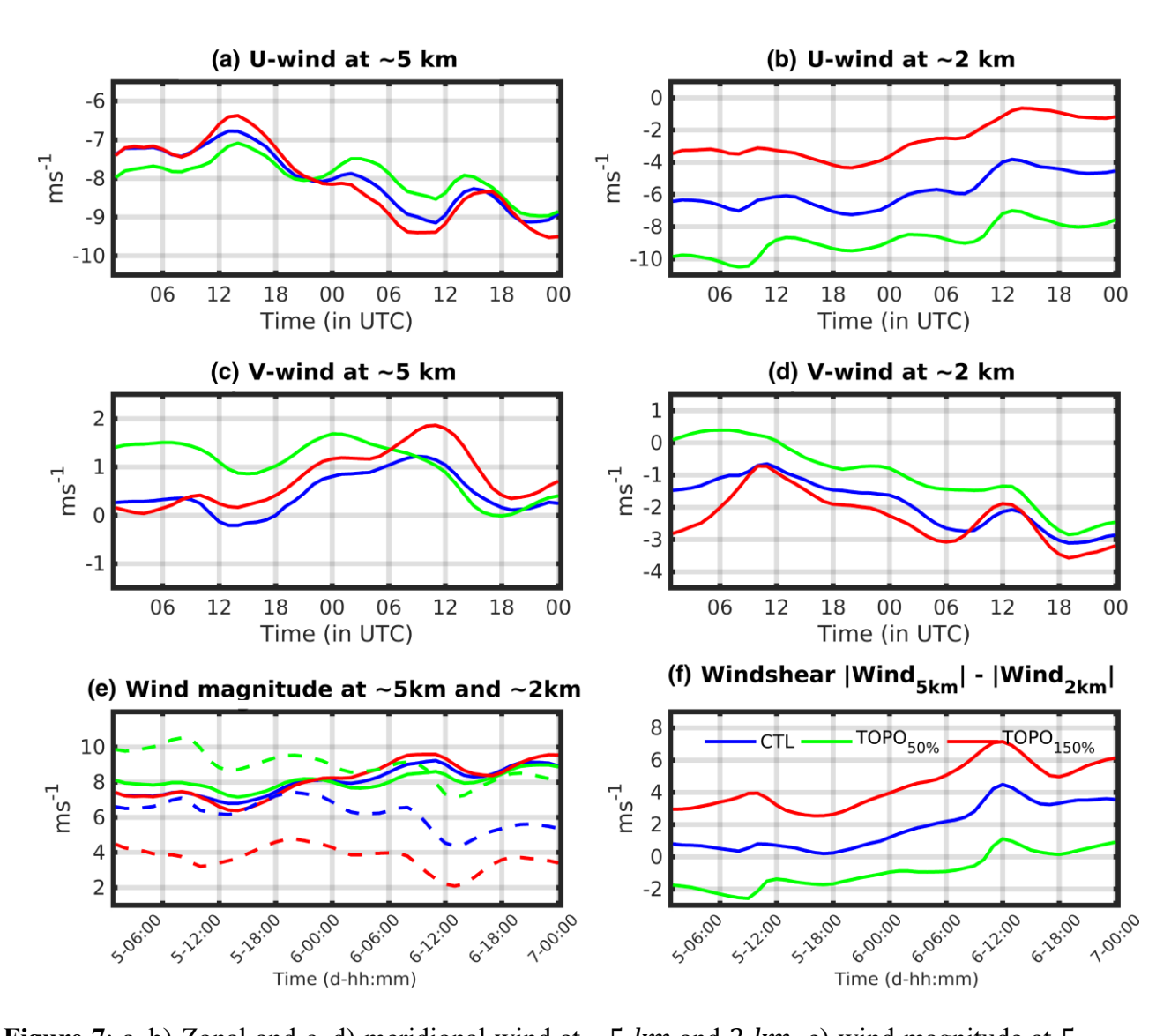


**Figure 7**: a–b) Zonal and c–d) meridional wind at  $\sim$ 5 km and 2 km, e) wind magnitude at 5 km (solid line) and 2 km (dashed line), and f) windshear. Data was spatially averaged between 5°N/S and 12 to 28°E and shown from 00:00 UTC on 05-Nov to 00:00 UTC on 07-Nov-2014.

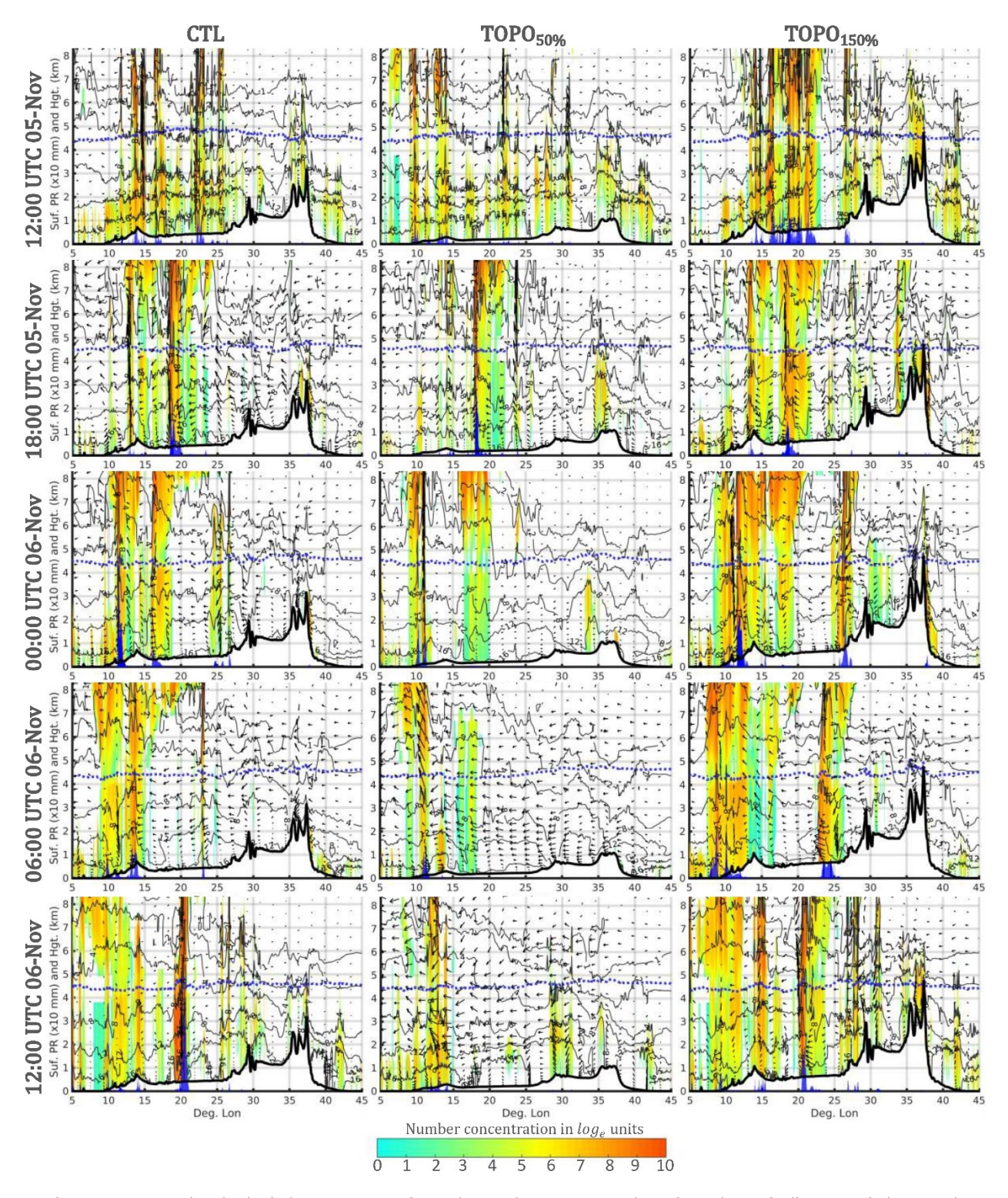


Figure 8: Longitude-height cross section along the equator showing the rain/ice particle number concentration (shaded), specific humidity ( $g kg^{*\%}$ ; grey contour), zonal and vertical wind (× 10) vector ( $ms^{*\%}$ ), the freezing level (dotted blue line), and rainfall (× 10 mm; blue bars along the x-axis) for the CTL,  $TOPO^{**}$ , and  $TOPO^{**}$  and  $TOPO^{**}$